Open Research Online

Noise-induced transitions in rugged energy landscapes

Journal Item

For guidance on citations see FAQs.

Version: Accepted Manuscript

oro.open.ac.uk

Noise-induced transitions in rugged energy landscapes

A. B. Duncan,[1,2] S. Kalliadasis,[2] G. A. Pavliotis,[1] and M. Pradas[3]

[1]*Department of Mathematics, Imperial College London, London SW7 2AZ, UK*

[2]*Department of Chemical Engineering,*

Imperial College London, London SW7 2AZ, UK

[3]*Department of Mathematics and Statistics,*

The Open University, Milton Keynes MK7 6AA, UK

Abstract

We consider the problem of an overdamped Brownian particle moving in multiscale potential with $N+1$ characteristic length scales: the macroscale and N separated microscales. We show that the coarse-grained dynamics is given by an overdamped Langevin equation with respect to the free energy and with a space dependent diffusion tensor, the calculation of which requires the solution of N fully coupled Poisson equations. We study in detail the structure of the bifurcation diagram for one-dimensional problems and we show that the multiscale structure in the potential leads to hysteresis effects and to noise-induced transitions. Furthermore, we obtain an explicit formula for the effective diffusion coefficient for a self-similar separable potential and we investigate the limit of infinitely many small scales.

I. INTRODUCTION

Brownian motion in disordered media (or rugged energy landscapes) is a problem of great scientific and technological interest, and applications are found in a wide range of different areas, such as e.g. collective transport of particles in random media [16, 17, 21, 36, 39, 41], molecular motors [27, 37], and protein reaction dynamics and folding [43], to name but a few. In the latter example in particular, proteins are dynamic macromolecules that exhibit many scales of molecular motion which is governed by a hopping mechanism through the local minima of the free-energy surface, the so-called conformational substrates or microstates. Understanding the effect of the microstates on the large scale dynamics of proteins is a problem of both theoretical and practical interest. At the same time, a rugged energy landscape can introduce metastability in the system [11, 12] and the degree of metastability can increase with the complexity of the landscape, invalidating predictions based on thermodynamic arguments, e.g. [50]. In addition, other systems characterised by the presence of rugged energy landscapes include flows in structured or disordered media such as fluid flow in porous media [51–53] or contact line dynamics on chemically and/or topographically heterogeneous substrates [46, 48–50, 57, 58]; while the understanding of conformational changes in complicated multiscale energy landscapes can have significant impact to technological applications such as crystallisation [56] and drug design [30].

The dynamics of a Brownian particle moving in a rugged energy landscape can be modeled using the Langevin dynamics, either non-Markovian [38, Ch. 8], underdamped or the overdamped (Smoluchowski) dynamics in a multiscale potential which can be taken to be either deterministic or random. The main goal of the present work is to study in detail the coarse-grained dynamics of the Smoluchowski dynamics in an N-scale periodic potential. In particular, we will derive rigorously the coarse-grained dynamics and study the quantitative and qualitative properties of the homogenized model. It is important to note that many interesting phenomena, such as subdiffusion, may arise in the coarse grained dynamics systems with a multiscale potential, and, as it was shown in [59], the presence of a microscale ("roughness") in the potential increases the mean first passage time. In particular, given a potential $V(x)$ with two metastable states, perturbing $V(x)$ with microscale fluctuations would result in a decrease in the escape/reaction rate between the two states, see also [22] (and a generalization of this would be finding the corresponding transition/relaxation

times [34, 35]). Such results can be obtained in a systematic and rigorous way using analytical multiscale techniques. One can also approximate the effective dynamics numerically, using methods such as heterogeneous multiscale methods [2], reduced basis finite element heterogeneous multiscale methods, [1], as well as equation-free methods [20, 24].

Here, we further assume an overdamped Langevin dynamics of a Brownian particle moving in a multiscale periodic potential, where the macroscale is assumed to be confining (see figure 1 for some examples of multiscale potentials). By carefully analysing the corresponding effective (averaged) equation in different examples of potentials we are able to observe nontrivial dynamics which emerges as a consequence of the interplay between noise level and microscopic structure. In particular, we find that the microscopic fluctuations conspire with the additive noise to produce noise-induced hysteresis and noise-induced stabilisation depending on the particular choice of the potential. In all cases, we are able to fully characterise the different state transitions in terms of critical exponents.

Our basic model will be the first-order Langevin equation

$$dX_t^\epsilon = -\nabla V_\epsilon \left(X_t^\epsilon \right) dt + \sqrt{2\sigma} dW_t, \tag{1}$$

where W_t denotes standard Brownian motion on $\mathbb{R}^d$ and where the magnitude of the noise intensity σ would typically be related to the inverse temperature. The potential depends on $N + 1$ scale, the macroscale and N small scales:

$$V_\epsilon(x) = V\left(x, \frac{x}{\epsilon}, \frac{x}{\epsilon^2}, \ldots \frac{x}{\epsilon^N} \right), \tag{2}$$

and it is assumed to be confining at the macroscale and periodic in all small scales (detailed assumptions on the potential will be presented in the next section). For the dynamics (1), with the potential (2) tools from homogenization theory, in particular reiterated homogenization [3] can be used in order to obtain an effective equation, valid in the limit of infinite scale separation $\epsilon \to 0$.

Several aspects of this problem have already been studied. First, for periodic potentials with one characteristic length scale, under the diffusive rescaling $X_t^\epsilon := \epsilon X_{t/\epsilon^2}$ the effective diffusive dynamics becomes diffusive with an effective diffusion matrix D that can be calculated by solving an appropriate Poisson equation, posed on the unit periodicity cell [42, Ch. 13], [9, Sec. 3.4]. This result is a form of the functional central limit theorem for diffusion processes with periodic coefficients [8]. Furthermore, diffusion is always depleted

3

and it becomes exponentially small in the limit $\sigma \to 0$ [25]. The case of Brownian dynamics in a two-scale separable potential was studied in [40]. In particular, the dynamics (1) with a potential V in (2) of the form $V(x, y; \alpha) = \alpha V(x) + p(y)$, with $p(\cdot)$ a smooth periodic function, was considered. It was shown in [40] that the maximum likelihood estimator for the coefficients in the drift of the homogenized equation, given observations from the full dynamics (1), is asymptotically biased.

On the other hand, the problem of homogenization for Brownian particles in periodic potentials with N−scales, in the absence of a macroscopic/confining potential was studied in [5, 33]. In these papers the overdamped Langevin dynamics in potentials of the form

$$V^N(x) = \sum_{k=1}^{N} U_k \left(\frac{x}{R_k} \right), \tag{3}$$

where U_k, $k = 1, \ldots$ are Hölder continuous periodic potentials. Under the assumption that the scale ratios $\frac{R_{k+1}}{R_k}$ are bounded from above and below (in particular, allowing the possibility of a lack of scale-separation), it was shown that the eigenvalues of the effective diffusivity tensor $D(V^N)$ decay exponentially quickly as the number of scales increases. Using this result, the authors were able to show that in the limit of infinitely many scales the effective behavior is characterized by anomalous slow behavior. This subdiffusive behavior can be analyzed in a quantitative way by studying the mean exit time of the effective dynamics from a ball whose radius is of $O(1)$.

The potential (2) that we consider here can be thought of as a caricature of a disordered medium. For self-similar potentials of the form

$$V_\epsilon(x) = \sum_{j=1}^{+\infty} V \left(\frac{x}{\epsilon^j} \right), \tag{4}$$

where $V(\cdot)$ is a periodic function, it is possible, at least in one dimension, to obtain an analytical formula for the effective diffusion coefficient.

Here we will show that the coarse-grained equation of (1) is reversible with respect to an appropriate Gibbs measure and that the effective potential is given by a coarse-grained free energy. In addition, an important point to note is that, even though the noise in the full dynamics (1) is additive (since it is due to thermal fluctuations) the noise in the coarse-grained model is multiplicative. It is well-known that multiplicative noise can lead to noise-induced state transitions, both first- and second-order [29]. The fact that additive

noise from the fast scales, combined with the multiscale nature of the dynamics, leads to multiplicative noise and noise-induced transitions in the coarse-grained dynamics, was shown rigorously and investigated in detail for the stochastic Kuramoto-Shivashinsky (sKS) equation–an SPDE with no gradient structure [45, 47]. Specifically, as was shown in these studies, the coarse-grained dynamics of the sKS equation near the instability threshold is described by a low-dimensional stochastic differential equation (SDE) (an "amplitude equation") of the Landau-Stuart type with additive as well as multiplicative noise. For particular choices of the spatial correlation structure of the noise, the amplitude equation contains only multiplicative noise that leads to noise-induced stabilization and intermittent behavior. The transition between the three possible states of the system–normal, Gaussian-like behavior, intermittency and stabilization–depends on the strength of the noise.

One of our goals here is to investigate similar issues for the multiscale overdamped Langevin dynamics. In particular, following the techniques developed in [29], see also [38, Sec. 5.4], for non-multiscale SDEs with multiplicative noise in one dimension, we analyze the effect of the multiscale structure on the bifurcation diagram of the coarse-grained dynamics in one dimension. In particular, we show that the presence of several spatial scales leads to hysteresis loops in the bifurcation diagram which we can characterize quantitatively in terms of an appropriate critical exponent. We note the similarities between our findings and the work on critical transitions and bifurcation theory for non-autonomous stochastic dynamical systems, in particular the emergence of hysteresis phenomena in the study of the so-called tipping points [26]. A similar numerical study of water molecules filling or emptying carbon nanotubes was investigated in [55], where a coarse grained potential energy landscape was derived computationally, using coarse-grained molecular dynamics, and use to investigate the metastability and hysteretic parameter dependence of the dynamics.

The rest of the paper is organized as follows: In Section II we present the model that we will be considering in detail and we also give our main results: the formula for the homogenized equation and the main properties of the effective potential (free energy) and of the effective diffusion tensor. The effect of the multiscale structure of the potential on a pitchfork bifurcation is studied in Section III. Noise-induced stabilization phenomena for multiscale potentials are considered in Section IV. In Section V we calculate the effective diffusion coefficient for a Brownian particle moving in a piecewise linear self-similar potential with infinitely many scales. Conclusions and a discussion are offered in Section VI and
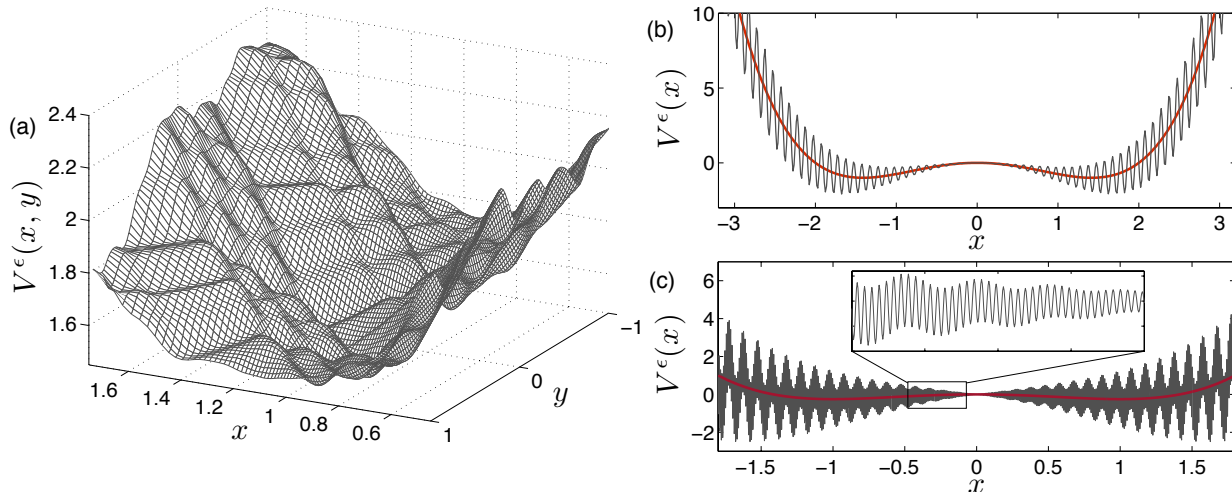
FIG. 1: (Color online) Examples of multiscale potentials. (a) A two-dimensional rough surface which corresponds to the interfacial energy of a droplet on a chemical heterogeneous substrate (see e.g. [57]). Panels (b) and (c) correspond to the case of a one-dimensional (1D) periodic multiscale potential given by (25) with $\alpha = 0.5$ (b) and (35) (c). The inlet of panel (c) is a zoom into the area marked by a rectangle.

the derivation of the coarse-grained equation and the calculation of the effective diffusion coefficient using multiscale techniques are outlined in the Appendices.

II. BROWNIAN MOTION IN A RUGGED ENERGY LANDSCAPE

We consider the overdamped Langevin dynamics in a multiscale potential with $N + 1$ characteristic length scales. The dynamics is given by the following SDE:

$$dX^\epsilon(t) = -\nabla V^\epsilon \left(X^\epsilon(t) \right) dt + \sqrt{2\sigma} dW(t), \tag{5}$$

where the potential $V^\epsilon(x)$ is of the form

$$V^\epsilon(x) = V\left(x, \frac{x}{\epsilon}, \frac{x}{\epsilon^2}, \ldots, \frac{x}{\epsilon^N} \right), \tag{6}$$

where $\epsilon \ll 1$ measures the degree of scale separation and where $V(x, y_1, \ldots, y_N)$ is a smooth function which is periodic in all but the first variable. The variables $y_1, \ldots, y_N$ characterise the microscopic scales of the potential while x represents the macroscale. So V is assumed to have a fractal-like structure which is realistic and allows for analytical progress to be made. Also, without loss of generality, we may also assume that V has period one in each

6

microscopic variable. $W(t)$ denotes standard Brownian motion in $\mathbb{R}^d$ and $\sigma > 0$ corresponds to the temperature. We shall assume that the potential can be decomposed as follows:

$$V(x, y_1, \ldots, y_N) = V_0(x) + V_1(x, y_1, \ldots, y_N), \tag{7}$$

where V_0 is assumed to be confining potential, while V_1 is assumed to be bounded uniformly with respect to all parameters, and periodic with period 1 with respect to the variables $y_1, \ldots, y_N$. This ensures that both the full dynamics (5) and the coarse-grained dynamics, (10) below, are ergodic [38, Sec. 4.5]. In particular, the process $\{X^\epsilon(t)\}$ is (exponentially) ergodic[60] with invariant distribution

$$\rho^\epsilon(x) = \frac{1}{Z^\epsilon} e^{-V\left(x, \frac{x}{\epsilon}, \frac{x}{\epsilon^2}, \ldots, \frac{x}{\epsilon^N}\right)/\sigma}, \quad Z^\epsilon := \int_{\mathbb{R}^d} e^{-V\left(x, \frac{x}{\epsilon}, \frac{x}{\epsilon^2}, \ldots, \frac{x}{\epsilon^N}\right)/\sigma} \, dx. \tag{8}$$

The dynamics $\{X^\epsilon(t)\}$ given by (5) is reversible with respect to the distribution (8). In particular, the generator of the process $\{X^\epsilon(t)\}$ is self-adjoint in the space $L^2(\mathbb{R}^d; \rho^\epsilon(x))$ and can be written in the form

$$\mathcal{L}^\epsilon \cdot = \frac{\sigma}{\rho^\epsilon(x)} \nabla \cdot \left(\rho^\epsilon(x) \nabla \cdot\right). \tag{9}$$

Introducing the auxiliary variables $y_n = \frac{x}{\epsilon^n}$, $n = 1, \ldots N$ and using the chain rule we can write (5) as a system of interacting diffusions across scales:

$$
\begin{aligned}
dX^\epsilon(t) &= -\nabla_x V(X^\epsilon(t), Y_1^\epsilon(t), \ldots, Y_N^\epsilon(t)) \, dt \\
&\quad - \sum_{\ell=1}^N \frac{1}{\epsilon^\ell} \nabla_{y_\ell} V(X^\epsilon(t), Y_1^\epsilon(t), \ldots, Y_N^\epsilon(t)) \, dt + \sqrt{2\sigma} \, dW(t), \\
dY_n^\epsilon(t) &= -\frac{1}{\epsilon^n} \nabla_x V(X^\epsilon(t), Y_1^\epsilon(t), \ldots, Y_N^\epsilon(t)) \, dt \\
&\quad - \sum_{\ell=1}^N \frac{1}{\epsilon^{n+\ell}} \nabla_{y_\ell} V(X^\epsilon(t), Y_1^\epsilon(t), \ldots, Y_N^\epsilon(t)) \, dt + \sqrt{\frac{2\sigma}{\epsilon^{2n}}} \, dW(t),
\end{aligned}
$$

for $n = 1, \ldots N$. The state space of the diffusion process $\{X^\epsilon(t), Y_1^\epsilon(t), \ldots Y_N^\epsilon(t)\}$ is $\mathbb{R}^d \times \mathbb{T}^d \times \cdots \times \mathbb{T}^d$ where $\mathbb{T}^d$ denotes the unit torus. This auxiliary diffusion process inherits from (5) the properties of ergodicity and reversibility. Our goal is to eliminate the fast scales $\{Y_1^\epsilon(t), \ldots Y_N^\epsilon(t)\}$ and to obtain a closed equation for the macroscopic variable $X(t)$. We remark on the similarity between this homogenization/coarse-graining problem and that of the derivation of a mean-field limit equation for interacting diffusions [15]. In Appendix A we use homogenization theory [42] and in particular the theory of reiterated homogenization [3] to derive such a closed, SDE for the macroscopic variable $X^\epsilon(t)$, valid in the limit of infinite

scale separation $\epsilon \to 0$. In this section we present the coarse-grained model and we elucidate some of its main properties. In particular, in Appendix A we derive the following result: the solution X_t^ϵ of (5) converges as $\epsilon \to 0$ to the solution of the SDE

$$dX_t = -\mathcal{M}(X_t)\nabla\Psi(X_t)\,dt + \nabla \cdot \mathcal{M}(X_t)\,dt + \sqrt{2\mathcal{M}(X_t)}\,dW_t, \qquad (10)$$

where $\Psi(x)$ denotes the free energy and $\mathcal{M}(x)$ the effective diffusion tensor:

$$\Psi(x) = -\ln Z(x), \quad Z(x) = \int_{\mathbb{T}^d} \cdots \int_{\mathbb{T}^d} e^{-V(x,y_1,\ldots,y_N)/\sigma}\,dy_N \ldots dy_1, \qquad (11)$$

and

$$\mathcal{M}(x) = \frac{\sigma}{Z(x)} \int_{\mathbb{T}^d} \cdots \int_{\mathbb{T}^d} (I + \nabla_{y_N}\theta_N) \cdots (I + \nabla_{y_1}\theta_1) e^{-V(x,y_1,\ldots,y_N)/\sigma}\,dy_N \cdots dy_1. \qquad (12)$$

The corrector fields $\{\theta_1(x),\ldots\theta_N(x)\}$ are defined recursively as follows: let θ_{N-k} be the solution of

$$\nabla_{x_{N-k}} \cdot (\mathcal{M}_{N-k}(x,y_0,\ldots,y_{N-k})(\nabla_{x_{N-k}}\theta_{x_{N-k}}(x,y_1,\ldots,y_{N-k}) + I)) = 0, \quad y_{N-k} \in \mathbb{T}^d, \ (13)$$

where for $1 \leq k < N$:

$$\mathcal{M}_{N-k}(x,y_1,\ldots,y_{N-k}) = \int_{\mathbb{T}^d} \cdots \int_{\mathbb{T}^d} (I+\nabla_N\theta_N) \cdots (I+\nabla_{N-k+1}\theta_{N-k+1}) e^{-V/\sigma}\,dy_N \ldots dx_{N-k+1}, \qquad (14)$$

and $\mathcal{M}_N(x,y_1,\ldots,y_N) = e^{-V(x,y_1,\ldots,y_N)/\sigma}I$. It is possible to show that the effective diffusion tensor is positive definite, uniformly in $x \in \mathbb{R}^d$ and to obtain upper and lower bounds on M.

The homogenized dynamics $X(t)$ is exponentially ergodic and reversible with respect to the invariant distribution

$$\rho(x) = \frac{Z(x)}{\overline{Z}}, \quad \overline{Z} = \int_{\mathbb{R}^d} Z(x)\,dx. \qquad (15)$$

The generator of the homogenized dynamics, which is a self-adjoint operator in $L^2(\mathbb{R}^d, \rho(x))$ can be written in the form

$$\mathcal{L}\cdot = \frac{1}{Z(x)}\nabla_x \cdot (Z(x)\mathcal{M}(x)\nabla_x\cdot). \qquad (16)$$

We remark that $\overline{Z}$ in (15) is the partition function of the full dynamics X_t^ϵ, Y_t^ϵ and requires the calculation of an integral over $\mathbb{R}^d \times \mathbb{T}^d$. It can be shown that invariant distribution of the homogenized dynamics is the weak limit of the invariant distribution (8) of $X^\epsilon(t)$. This follows from properties of periodic functions [13, Ch. 2].

The coarse-grained equation (10) that we derive here provides us with a rigorous derivation of the free energy (11) for systems with strong scale separation which can be used, in turn, to compute equilibrium coarse-grained quantities [10]. On the other hand, the homogenized dynamics (10) is the most general form of a reversible diffusion process with respect to the invariant distribution (15), see [38, Sec 4.6] and can be used to study time-dependent phenomena such as bifurcations and noise-induced transitions. Indeed, an important point to note is that for the case of nonseparable potentials, as given by (6), all scales are fully coupled in the hierarchy of Poisson equations (13)-(14). As a result of this, even through the noise in the original dynamics (5) is due to thermal fluctuations and is hence additive, the noise in the coarse-grained dynamics is multiplicative, something which, as it is well known and as was emphasized in the Introduction, can lead to noise-induced transitions [29]. These points will be elucidated in Sections III and IV.

A final remark is that the noise in the coarse-grained dynamics becomes additive when the potential (6) is separable, i.e.

$$V^\epsilon(x) = \sum_{n=0}^{N} V_n \left(\frac{x}{\epsilon^n} \right), \tag{17}$$

(a potential that could be achieved by design in a physical setting, and hence also realistic), a surprising result and perhaps counterintuitive as one might expect that coarse graining always leads to multiplicative noise in the effective description. In this case, the Poisson equations (13)-(14) can be solved in a hierarchical fashion, and the homogenized equation is of the form (10), but with a constant effective diffusion tensor. For illustrative purposes we present the formulas for $N = 1$ [40], in which case the effective dynamics is given by the SDE:

$$dX_t = -\mathcal{M}\nabla V_0(X_t)\, dt + \sqrt{2\sigma\mathcal{M}}\, dW_t, \tag{18}$$

where

$$\mathcal{M} = \int_{\mathbb{T}^d} (I + \nabla_y \theta(y)) (I + \nabla_y \theta(y))^T \, \mu(dy) \tag{19}$$

and

$$\mu(dy) = \rho(y)dy = \frac{1}{Z} e^{-\sigma^{-1} V_1(y)}\, dy, \quad Z = \int_{\mathbb{T}^d} e^{-\sigma^{-1} V_1(y)}\, dy. \tag{20}$$

The field $\phi(y)$ is the solution of the Poisson equation

$$-\mathcal{L}_0 \theta(y) = -\nabla_y V_1(y), \quad \mathcal{L}_0 := -\nabla_y V_1(y) \cdot \nabla_y + \sigma \Delta_y, \tag{21}$$

with periodic boundary conditions.

A. The homogenized equation in 1D

It is well known that homogenized coefficients in 1D can be computed explicitly, up to quadratures [42, Sec. 12.6.1, Sec. 13.6.1]. This is the case for the $N-$scale homogenization problem that we consider in this study. In Appendix B we show how, by solving the family of Poisson equations in (13)-(14) and by using formula (12) we obtain the following formula for the effective diffusion coefficient

$$\mathcal{M}(x) = \frac{\sigma}{Z_+(x)Z_-(x)}, \quad Z_\pm(x) = \int_{\mathbb{T}^N} e^{\mp V(x,y_1,\dots,y_N)/\sigma} dy_1 \dots dy_N, \tag{22}$$

see also [59]. Of course, the explicit calculation of the effective diffusion coefficient in one dimension using (22) requires the calculation of the partition functions $Z_\pm(x)$. In Section V we show how these multiple integrals can be calculated analytically for the case of an $N-$scale potential that is piecewise linear at all scales.

In the following sections we will consider different examples of multiscale potentials in one dimension to study the interplay between noise and the multiscale structure of the potential. Our goal, in particular, is to understand how the microscopic fluctuations can affect the global dynamics of the system.

III. A PITCHFORK BIFURCATION: NOISE-INDUCED HYSTERESIS

Consider the following SDE:

$$dX(t) = (\alpha X(t) - X(t)^3)dt + \sqrt{2\sigma}dW(t), \tag{23}$$

the deterministic part of which is the normal form for a supercritical pitchfork bifurcation. For $\alpha < 0$ there is a single stable equilibrium at 0 while for $\alpha > 0$ there is an unstable equilibrium at $x = 0$ and two stable equilibria at $x = \pm\sqrt{\alpha}$. The system described by (23) has a potential $V_0(x;\alpha) = -\frac{\alpha}{2}x^2 + \frac{1}{4}x^4$.

We define a two-scale potential by introducing a rapid fluctuation on the bifurcation parameter α so the potential reads:

$$V(x,y;\alpha) = \frac{1}{4}x^4 - \left[\frac{\alpha + g_\delta(x)\sin(2\pi y)}{2}\right]x^2, \tag{24}$$

which in turn can be rewritten as:

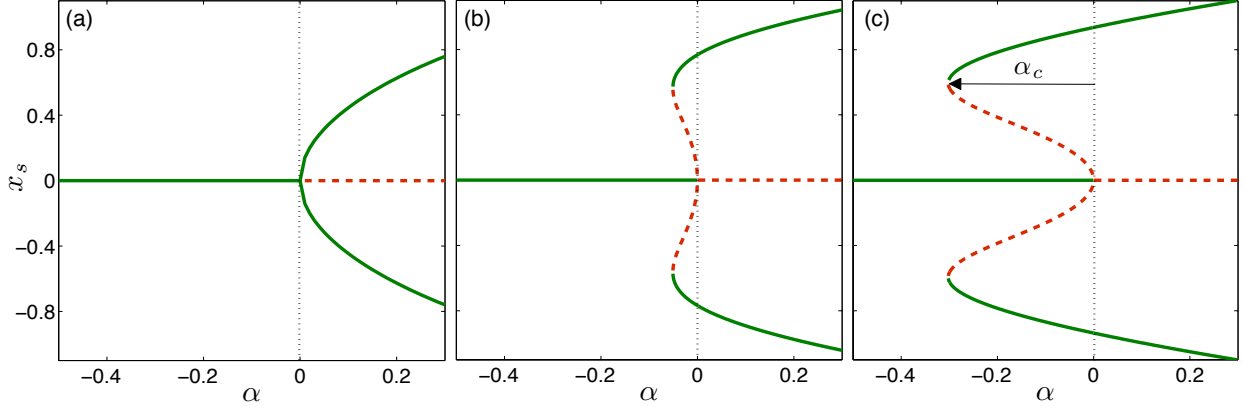$$V(x,y;\alpha) = V_0(x;\alpha) - \frac{1}{2}g_\delta(x)x^2\sin(2\pi y), \tag{25}$$

FIG. 2: Bifurcation diagram of the two-scale potential given by (25) obtained by solving (27) for (a) $\sigma = 0.5$, (b) $\sigma = 0.2$, and (c) $\sigma = 0.1$.

where we have introduced a decaying function with the properties $g_\delta(0) = 1$ and $g_\delta(x \gg \delta) \to 0$. Note that the main purpose of this function is to ensure that the microscopic fluctuations are confined within the region in which the macroscopic potential varies. An illustation of the above potential for the case of $\alpha = 0.5$ is shown in figure 1.

We start by studying the equilibrium properties of (23). The ergodic distribution of the homogenised dynamics is given by (15), which after including the potential given by (25), we obtain:

$$\rho(x) = \frac{1}{Z} e^{-V_0(x;\alpha)/\sigma} I_0 \left(\frac{g_\delta x^2}{2\sigma} \right), \tag{26}$$

where $I_0(\cdot)$ is the modified Bessel function of the first kind which depends on both the position x and the noise intensity σ, and it is a correcting term coming from the microscopic fluctuations—note that if $g_\delta = 0$ we recover the Gibbs measure of the unpertubed macroscopic system. Therefore, we can see that the microscopic fluctuations are able to modify the equilibrium points of the system (i.e. the maxima of $\rho(x)$) and these are controlled by the noise intensity.

To quantify this effect, we construct the bifurcation diagram of the solution for different values of σ. To this end we look at the equilibria x_s of the above function $\rho(x)$ which are given by the solution of the following equation:

$$-x_s^3 + x_s \left[\alpha + \frac{I_0'(x_s^2 g_\delta / 2\sigma)}{I_0(x_s^2 g_\delta / 2\sigma)} \right] = 0. \tag{27}$$

The results are presented in figure 2 where we can see that for sufficiently large values of the noise level, the long-time behaviour of the macroscopic system demonstrates the same

11

qualitative behaviour as the unperturbed case with a *supercritical* pitchfork bifurcation occurring when $\alpha = 0$ [cf. Figure 2(a)]. However, as the noise intensity decreases, the behaviour becomes qualitatively different. Indeed, for some critical value of σ the pitchfork bifurcation becomes *subcritical* and two saddle-node bifurcations symmetric about the x-axis arise along the negative axis, giving rise to three stable and two unstable branches. As α passes 0 the central stable branch becomes unstable [cf. Figs. 2(b,c)]. In this scenario, we can identify three different dynamic states: (I) for $\alpha < \alpha_c < 0$ zero is a stable solution of the system, (II) for $\alpha_c < \alpha < 0$, in addition to zero, there are two other non-zero stable solutions, and (III) for $\alpha > 0$, zero becomes unstable and there are two non-zero stable solutions. We note that this system gives rise to a *hysteresis* loop and the macroscopic system will not follow the same equilibrium branch for α increasing as when α is decreased.

To further illustrate the transitions that arise in our multiscale system, we simulate the evolution of a Brownian motion in the two-scale potential (25). We choose $\sigma = 0.1$, $\epsilon = 0.1$ and g_δ to be a smooth mollification of the indicator function over $[-10, 10]$. We approximate the SDE numerically using a standard Euler-Maruyama discretisation with step size $\Delta t = 10^{-4}$. In Figure 3 we plot histograms generated from 10 independent runs each of 10^9 timesteps, for $\alpha = -0.5$, -0.25 and 0.25, respectively. The choices of α correspond to the dynamics before the bifurcation point, close to bifurcation point and after bifurcation, respectively, as illustrated in the bottom panel of figure 3. They correspond to the three dynamical states defined above. In each case, the red line denotes the exact stationary distribution $\rho(x)$ given by (26). The thin gray line denotes a normalized histogram, generated from the samples lying in $[-2, 2]$ with the size of each bin taken to be 0.05. We see that the approximated density exhibits large fluctuations around $\rho(x)$. This is to be expected since the stationary density $\rho^\epsilon(x)$ does not converge pointwise to $\rho(x)$, but only in the weak sense. Indeed, increasing the size of the histogram bins 0.1, as depicted by the dashed blue line, we see much better agreement in each case.
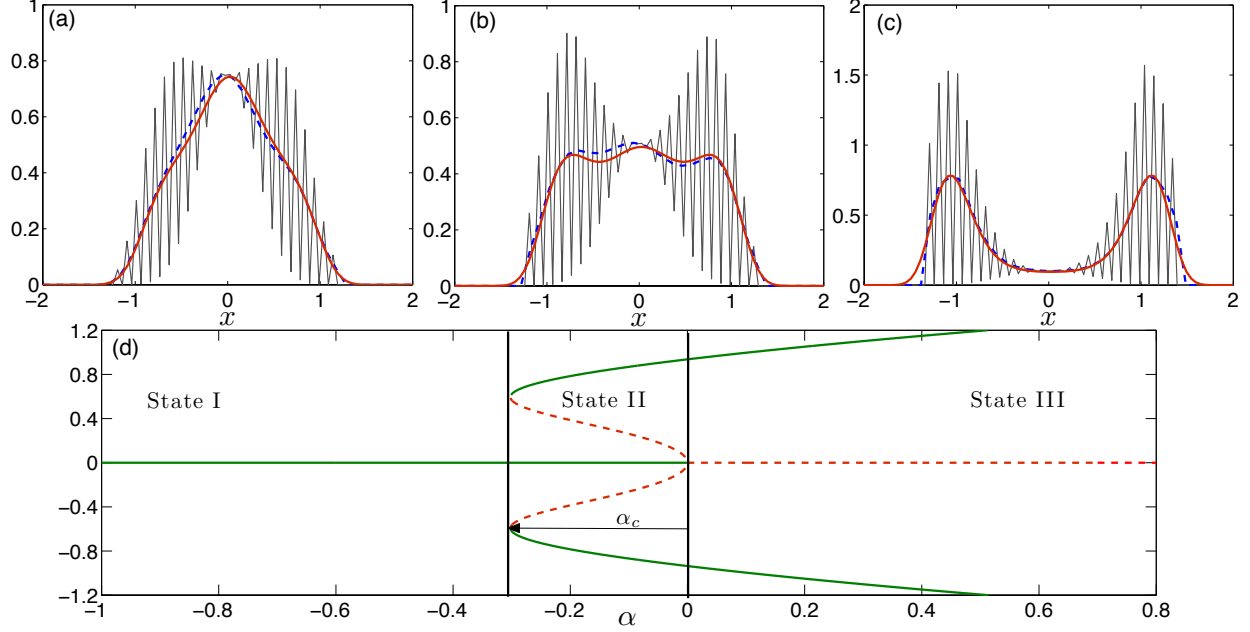
FIG. 3: (Color online) Top panels show histograms generated over a long sample of the SDE (23) with the two-scale potential (25) with $\sigma = 0.1$, $\epsilon = 10^{-1}$, and using bins of size 0.05 (thin gray line) and 0.1 (dashed blue line), for the three different dynamical states: (a) State I with $\alpha = -0.5 < \alpha_c$, (b) state II $\alpha = -0.25 \in [\alpha_c, 0]$, and (c) state III with $\alpha = 0.25 > 0$. In all three panels, the thick red line shows analytical homogenised solution given by (26). Panel (d) shows the corresponding bifurcation diagram for reference with the three states demarcated with vertical solid lines.

A. Extension to N scales

A natural extension in the two-scale potential of (25) is to add more microscopic scales, say up to N, so that the new potential is of the form:

$$V(x, y; \alpha) = V_0(x; \alpha) - \frac{1}{2} g_\delta(x) x^2 \sum_{n=1}^{N} \sin(2\pi y_n). \tag{28}$$

for $y_n = x/\epsilon^n$. In this case, the stationary distribution reads:

$$\rho(x) = \frac{1}{Z} e^{-\beta V_0} \left[I_0\left(\frac{x^2 g_\delta}{2\sigma} \right) \right]^N, \tag{29}$$

and (27) becomes:

$$-x_s^3 + x_s \left[\alpha + N \frac{I_0'(x_s^2 g_\delta/2\sigma)}{I_0(x_s^2 g_\delta/2\sigma)} \right] = 0. \tag{30}$$
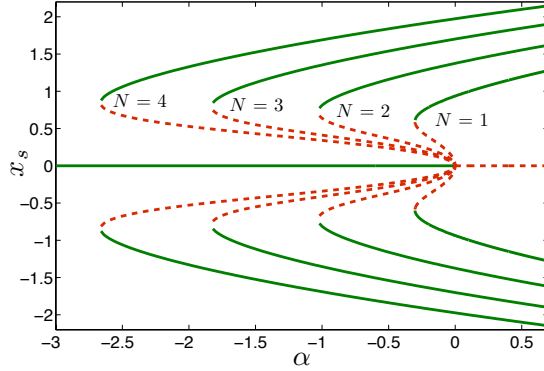
13

FIG. 4: Bifurcation diagram for different values of the number of microscopic scales $N = 1, 2, 3, 4$ (from left to right) in the potential defined in (28).
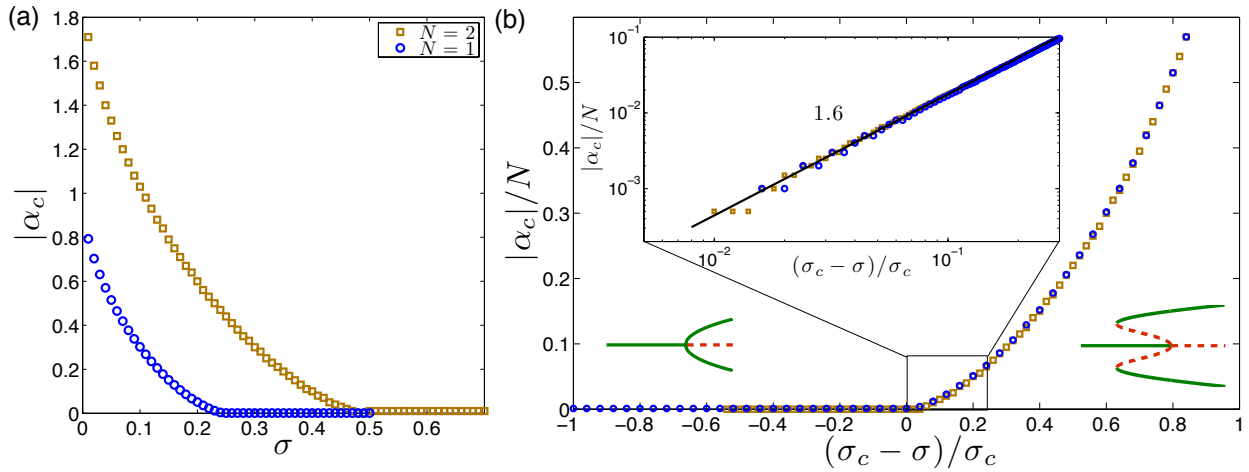

FIG. 5: Results obtained by using the multiscale potential defined in (28). (a) Transition from supercritical ($|\alpha_c| = 0$) to subcritical ($|\alpha_c| > 0$) as the noise intensity is decreased. (b) Rescaled σ and $|\alpha_c|$ show data collapse into a single curve. The inlet shows a log-log plot where we can identify a power-law behaviour close to criticality with exponent $\gamma = 1.6$. The corresponding bifurcation diagrams for the supercritical and subcritical cases are also shown for reference.

By computing again the equilibrium points and constructing the corresponding bifurcation diagram, we observe that the transition from supercritical to subcritical is in fact enhanced with the number of scales N (see figure 4 for the case with $\sigma = 0.1$).

To quantify the transition from a supercritical to a subcritical pitchfork bifurcation observed when the noise intensity is decreased (cf. figure 2), and how this depends on the number of microscopic scales N, we take the absolute value of α_c defined in the bottom panel
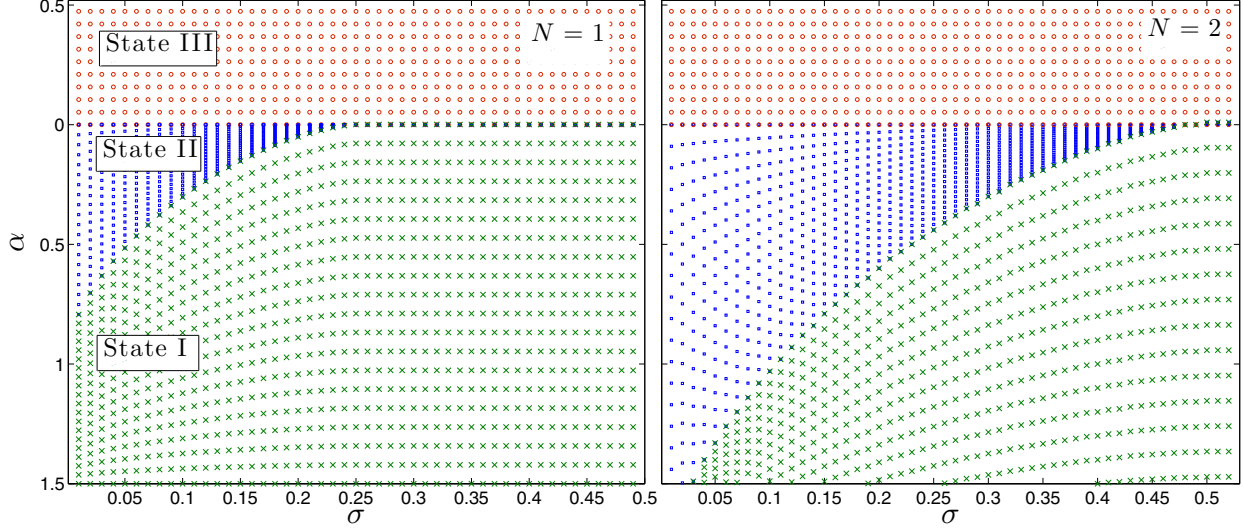
14

FIG. 6: Phase diagram showing the three dynamical states I (green) , II (blue), and III (red), which are observed in the potential given in (28) and defined in figure 2 for two values of the number of microscopic states N.

of figure 3 to play the role of an order parameter of the transition, such that the bifurcation is supercritical for $|\alpha_c| = 0$ and subcritical for $|\alpha_c| > 0$. The results are depicted in figure 5(a), where we can observe that $|\alpha_c|$ becomes zero at some critical value σ_c which depends on the number of microscopic scales. Indeed, by considering values of $x_s \ll 1$ in (30), we can expand the Bessel functions $(I_0'(x)/I_0(x) \sim x/2$ for $x \ll 1)$ and we can see that the two non-zero solutions exist for values of σ which are below the critical value:

$$\sigma_c = \frac{N}{4}, \tag{31}$$

which defines the critical point. By taking now the rescaled variables:

$$X \equiv \frac{\sigma_c - \sigma}{\sigma_c}, \qquad Y \equiv \frac{|\alpha_c|}{N}, \tag{32}$$

we can observe that all data collapse into a single curve, and close to critical point the transition is characterized by a power-law behaviour:

$$Y \sim |X|^\gamma, \tag{33}$$

with $\gamma = 1.6$ [cf. figure 5(b)]. In addition, we present in figure 6 a phase diagram on the plane (σ, α) where we can see how the different dynamical states (I), (II), and (III) defined

15

above depend on the number of microscopic scales N.

The manifestation of hysteresis in disordered systems at low temperatures (i.e. small σ) is well known. Indeed, a similar phenomenon is observed in the Ising model of a ferromagnetic material subject to an external magnetic field, where for temperatures lower than a critical temperature T_c, the mean spin of the system exhibits hysteresis as the magnitude of the external field is varied. This scenario is very much analogous to the model described in (23) and (25), where the parameter α controls the strength of an external perturbation, and for which hysteresis occurs only where the noise intensity σ is below a critical threshold. More generally, the observation that roughness of the energy landscape can give rise to hysteresis effects has been observed in various systems, for example hysteresis of contact angles at the solid-liquid interface of fluids wetting rough surfaces [14, 46, 49, 58], hysteresis in loading and unloading of rough adhesive surfaces [23] as well as folding-unfolding hysteresis in proteins with complex energy landscapes [4].

IV. NOISE-INDUCED STABILIZATION

As one would expect, the manner in which the multiscale pertubation of the potential will influence the equilibrium behaviour of X_t^ϵ depends strongly on the nature of the coupling between the the different scales in the energy potential. In particular, by introducing a perturbation of the potential at a third lengthscale, the long term dynamics of the diffusion process will be significantly altered. To this end, we now consider a tilted three-scale quartic potential of the form:

$$V(x, y_1, y_2; \alpha) = \frac{1}{4}x^4 - \left[\frac{\alpha + g_\delta \sin(2\pi y_1)}{2}\right]x^2 + g_\delta \lambda \sin(2\pi y_2)x. \tag{34}$$

which we rewrite as:

$$V(x, y_1, y_2; \alpha) = V_0(x; \alpha) - \frac{1}{2}g_\delta x^2 \sin(2\pi y_1) + g_\delta \lambda x \sin(2\pi y_2). \tag{35}$$

An example of this potential is shown in figure 1. The parameter λ above has been introduced to connect it with the potential presented in the previous section which is recovered when $\lambda = 0$. As before, we start by looking at the stationary distribution which we find to be:

$$\rho(x) = \frac{1}{Z}e^{-\beta V_0}I_0\left(\frac{x^2 g_\delta}{2\sigma}\right)I_0\left(\frac{x g_\delta \lambda}{\sigma}\right). \tag{36}$$
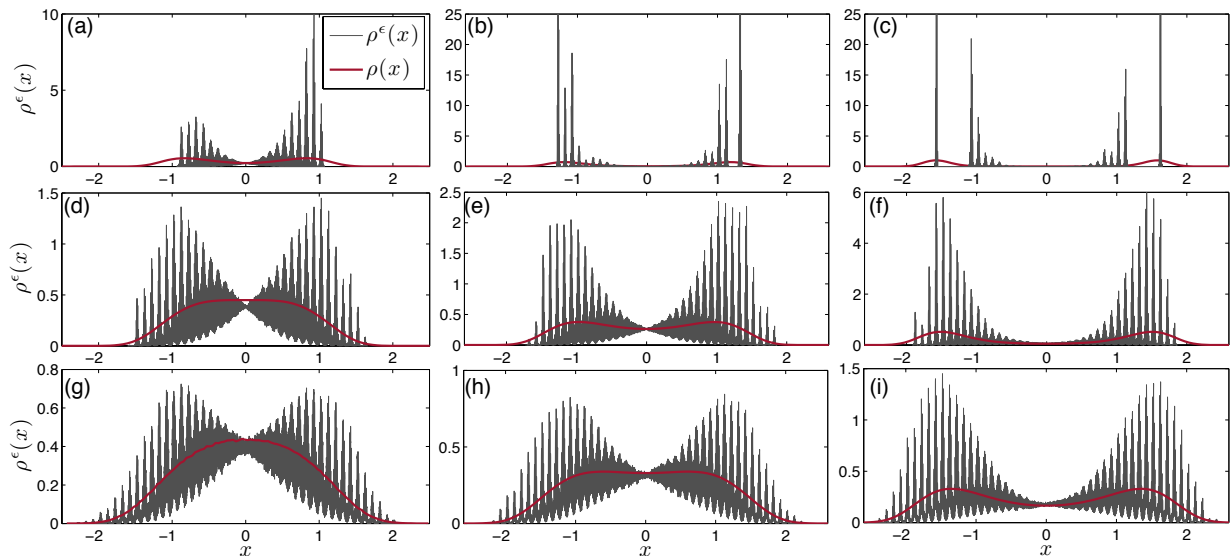
FIG. 7: Numerical solution of the stationary distribution $\rho^\epsilon(x)$ by solving the multiscale SDE with the potential given in (35) and the analytical solution $\rho(x)$ given by (36) (solid red line) for different values of the noise strength and the parameter α. (a), (b), and (c) correspond to $\sigma = 0.2$ for $\alpha = -1$, -0.2 and 1, respectively. (d), (e), and (f) correspond to $\sigma = 0.5$ for $\alpha = -1$, -0.2 and 1, respectively; and (g), (h), and (i) correspond to $\sigma = 1$ for $\alpha = -1$, -0.2 and 1, respectively.

Figure 7 shows numerical computations of both the stationary distribution obtained by solving the multiscale SDE with the potential given in (35) and the above analytical solution $\rho(x)$ for different values of σ and α, observing an excellent agreement in all cases. In addition, we look at the equilibria of $\rho(x)$ which are given by the following equation:

$$-x_s^3 + x_s \left[\alpha + \frac{I_0'(x_s^2 g_\delta / 2\sigma)}{I_0(x_s^2 g_\delta / 2\sigma)} \right] + \lambda \frac{I_0'(x_s g_\delta \lambda / \sigma)}{I_0(x_s g_\delta \lambda / \sigma)} = 0, \tag{37}$$

from which we construct the bifurcation diagram, shown in figure 8 for different values of the noise level σ. It is interesting to note that the introduction of the additional multiscale fluctuations in (35) gives rise to a significantly altered bifurcation structure. Indeed, the transition to subcritical bifurcation is not observed but rather the supercritical pitchfork bifurcation is being shifted to the left as the noise intensity is decreased. Moreover, it is remarkable that the macroscopic unperturbed behaviour is only recovered for sufficiently large values of σ. To make this statement more precise, we look at the value of α_0 which is defined as the value where the pitchfork bifurcation occurs (see figure 8) and which satisfies
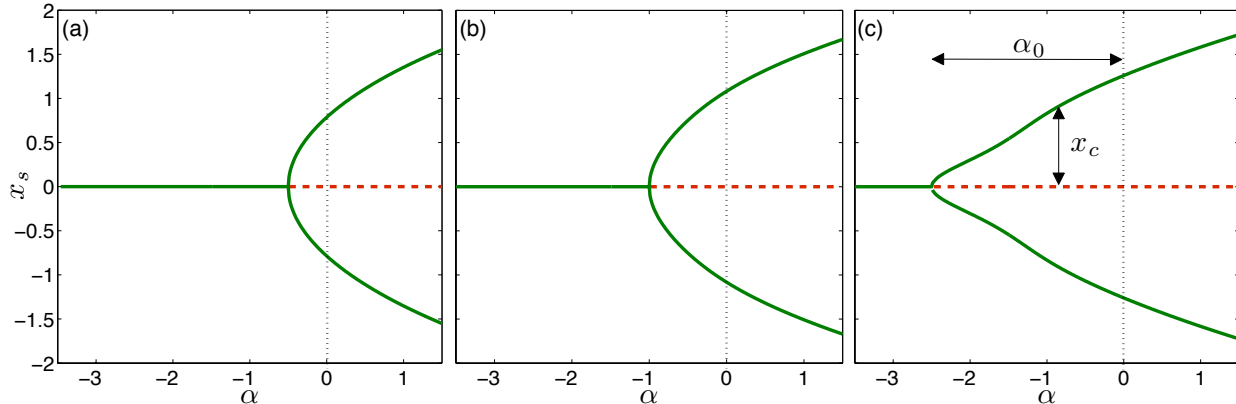
17

FIG. 8: Bifurcation diagram for the three-scale potential and for three different values of the noise strength, namely $\sigma = 0.2$ (a), $\sigma = 0.5$ (b), and $\sigma = 1$ (c).

the following condition:

$$\partial_x^2 \rho(x; \alpha_0)|_{x=0} = 0, \tag{38}$$

giving rise to:

$$\alpha_0 = -\frac{\lambda}{2\sigma}. \tag{39}$$

We hence conclude that for the three-scale potential, the case $\alpha_0 = 0$, which corresponds to the standard supercritical bifurcation, is only achieved when $\sigma \to \infty$ [we note also that for the unperturbed macroscopic dynamics ($g_\delta = 0$) and for the case of a two-scale potential analyzed in the previous section, $\lambda = 0$, we have $\alpha_0 = 0$ independently of σ].

An important consequence of the fact that α_0 depends on σ is that the stability of the zero solution can be tuned by changing the noise strength. Indeed, if we take a fixed (negative) value α, the zero solution will be unstable for values of σ which are below the critical value:

$$\sigma_c = \frac{\lambda}{2|\alpha|}, \tag{40}$$

and stable otherwise. How this transition is approached as we increase the value of σ can be studied by looking at the position of the local maximum, say x_c, of the stationary distribution $\rho(x)$ which is a solution of (37) [see figure 8(c) for the definition of x_c for a given value of α]. For a fixed value of α we then have that the zero solution is stable when $x_c = 0$ and unstable when $x_c > 0$. We can therefore define x_c to be the order parameter of this transition. Figure 9 shows how the position of one of the two maxima of the PDF approaches the value of zero as σ is increased and for different values of the chosen α, where we can see that near the
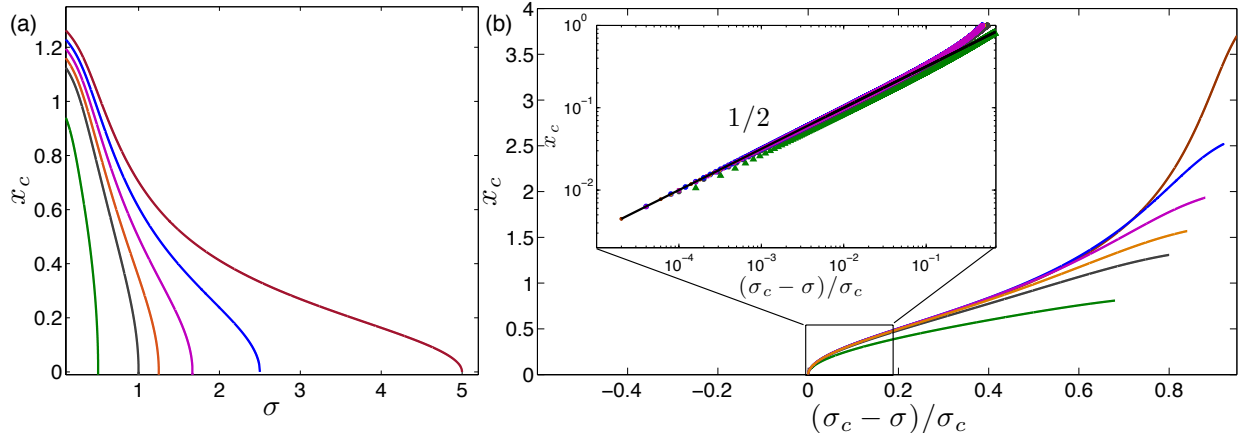
18

FIG. 9: (a) Position x_c of the local maximum of the PDF as function of the noise strength σ for different values of the parameter α, namely $\alpha = -1, -0.5, -0.4, -0.3, -0.2, -0.1$ (curves from left to right). Panel (b) shows the position of the maximum with respect to the the rescaled variable $(\sigma_c - \sigma)/\sigma_c$. When the solution is plot in a log-log scale (inlet panel) we can observe a power-law behaviour with exponent $1/2$.

critical point the solution exhibits a power-law behaviour of the form:

$$x_c \sim |X|^\gamma, \tag{41}$$

with $\gamma = 1/2$. Indeed, we can verify this behaviour analytically if we look at the solutions given by (37) in the limit of $x_c \ll 1$ for which we can expand the Bessel functions $[I_0'(x)/I_0(x) \sim x/2$ for $x \ll 1]$. Expanding around the critical point $\sigma = \sigma_c - \delta\sigma$ yields to leading order in $\delta\sigma$ that $x_c \sim |\delta\sigma/\sigma_c|^{1/2}$.

V.   BROWNIAN MOTION IN A PIECEWISE LINEAR SELF-SIMILAR POTENTIAL

In this section, we consider a piecewise-linear N-scale separable potential given by

$$V^\epsilon(x) = V_N\left(\frac{x}{\epsilon}, \ldots, \frac{x}{\epsilon^N}\right) = S\left(\frac{x}{\epsilon}\right) + S\left(\frac{x}{\epsilon^2}\right) + \ldots + S\left(\frac{x}{\epsilon^N}\right), \tag{42}$$

where

$$S(x) = \begin{cases} 2x & \text{if } x \bmod 1 \in [0, \frac{1}{2}); \\ 2 - 2x & \text{if } x \bmod 1 \in [\frac{1}{2}, 1), \end{cases} \tag{43}$$

for fixed $N \in \mathbb{N}$ and $\epsilon > 0$. Since we are dealing with a separable potential with no large-scale component, we know from the results presented in Section II that the coarse-grained

19

dynamics is purely diffusive, i.e. the coarse-grained Fokker-Planck equation is the heat equation:

$$\frac{\partial F_0(x,t)}{\partial t} = M(\sigma)\frac{\partial^2 F_0(x,t)}{\partial x^2}, \tag{44}$$

where M is a constant effective diffusion tensor. Since the fast scale fluctuations in the potential are separated, as it is described in B we can easily obtain the constant effective diffusion from (B2):

$$
\begin{aligned}
M(\sigma) &= \sigma \left(\int_{\mathbb{T}} e^{-S(z)/\sigma}\, dz \cdot \int_{\mathbb{T}} e^{S(z)/\sigma}\, dz \right)^{-N} \\
&= \sigma \left[\sigma^2 \left(1 - e^{-1/\sigma} \right) \cdot \left(e^{1/\sigma} - 1 \right) \right]^{-N} \\
&= \frac{\sigma}{\left[2\sigma^2 \left(\cosh\left(\frac{1}{\sigma}\right) - 1 \right) \right]^N}.
\end{aligned}
\tag{45}
$$

The N-scale perturbations have a retarding effect on the motion which is amplified as N increases, a consequence of the increased complexity of the potential. This is captured in the scalar term $K_N(\sigma) = \left[2\sigma^2 \left(\cosh\left(\frac{1}{\sigma}\right) - 1 \right) \right]^{-N}$, which is plotted in figure 10(a) for varying σ and for different values of N. We can see that, for each N, there is a neighbourhood up to some finite value σ_c where it is vanishingly small, say $K_N(\sigma) < \kappa$ with κ being an arbitrary small value. For σ outside this region, this coefficient rapidly transitions to the value 1, implying that the overdamped Brownian motion is no longer inhibited by the multiscale fluctuations. It is well known that Brownian motion in disordered media, in particular, fractal-like media can be anomalously slow. Classical examples include diffusion on the Sierpinski Carpet [7] and diffusions on comb-like structures [44]. In the physics literature, the association of renormalization on multiple scales with anomalous dynamics is well known and has been studied in various works, for example [54] where the anomalous electric properties of fluid-saturated sedimentary rocks were studied and [6], where a rigorous iterated effective medium approximation theory was developed and applied to study the conductivity of various composite materials.

As can be seen in figure 10(a), increasing the number of scales N moves this transition point to higher σ. One can estimate such a transition point by expanding the function $\cosh\left(\frac{1}{\sigma}\right) = 1 + \frac{1}{2}\frac{1}{\sigma^2} + \frac{1}{4!}\frac{1}{\sigma^4} + O(\sigma^{-6})$ so that at the transition point σ_c we have:

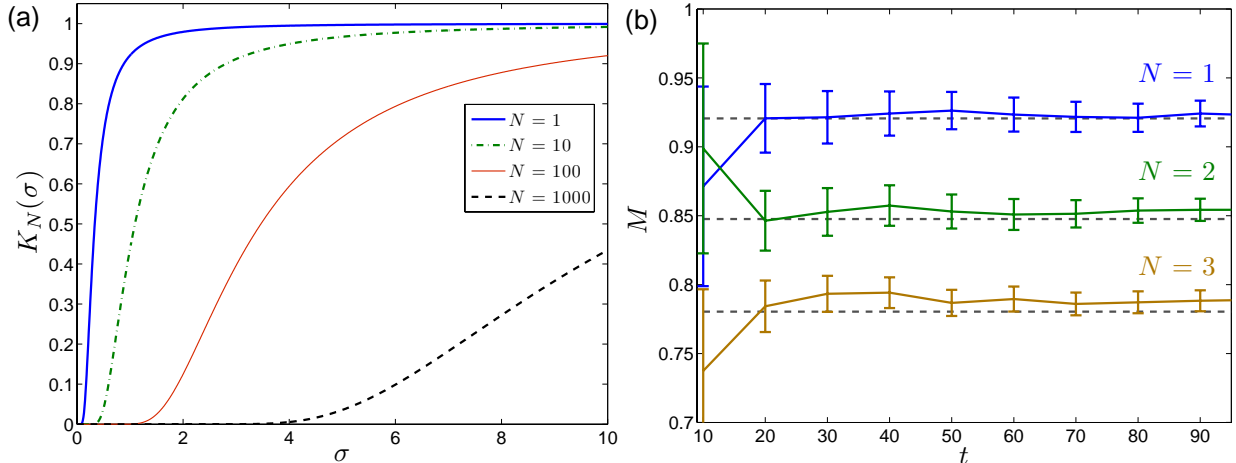$$K_N(\sigma_c) \sim \frac{1}{\left(1 + \frac{1}{12}\frac{1}{\sigma_c^2} \right)^N}. \tag{46}$$

20

FIG. 10: (a) Plot of the retardation factor $K_N(\sigma)$ over σ for different values of N. (b) Effective diffusion coefficient approximated from numerical simulations for $N = 1$, 2 and 3 compared to the homogenized diffusion coefficient $M(\sigma)$ predicted by (45) (dashed lines).

We are interested in finding the value of σ_c for which $K_N(\sigma_c) = \kappa$. By taking the logarithm of the above expression we obtain at leading order:

$$\sigma_c(N) \sim \frac{1}{\sqrt{12|\log \kappa|}} N^{1/2}, \tag{47}$$

which is valid for sufficiently large values of N.

To further demonstrate the effect of the scales on the rate of diffusion of $X^\epsilon(t)$, we numerically simulate (5) for the piecewise potential (42) for different values of N. For $\epsilon = 0.1$ and $\sigma = 1$, we approximate the solution of (5) up to time $T = 100$, using an Euler-Maruyama discretisation with step-size varying between 10^{-7} and 10^{-8}. Given the resulting approximation $X_1, X_2, \ldots, X_M$, the diffusion coefficient was approximated by using the maximum likelihood estimator:

$$\hat{D}(\{X_1, \ldots, X_M\}) = \frac{1}{\lfloor M/k \rfloor} \sum_{i=1}^{\lfloor M/k \rfloor} \frac{(X_{i+k} - X_i)^2}{2k\Delta t}, \tag{48}$$

where $k \in \mathbb{N}$ controls the subsampling time $\delta = k\Delta t$. As noted in [40], when inferring transport coefficients from multiscale data, the subsampling rate must be chosen carefully to ensure that the estimator converges to the diffusion coefficient of (5) on the $O(1)$ timescale (i.e. the effective diffusion coefficient). Based on short numerical experiments, $k = 10^{-1}/\Delta t$ was used. The estimator (48) was then averaged over 100 independent realisations. In figure

21

10(b) we show the average of this estimator over 100 realisations, as a function of time, for $N = 1$, $N = 2$ and $N = 3$ scales respectively. The error bars denote 95% confidence intervals. The dashed lines denote the homogenized effective diffusion coefficient $M(\sigma)$ predicted by (45). We see good agreement in each case, although the discrepancy between the simulated diffusion coefficient and $M(\sigma)$ increases as N increases. This discrepancy is likely caused by discretisation error due to the increase in stiffness for larger values of N, as well as the fact that the small scale parameter ϵ might not be sufficiently small to faithfully capture the homogenized dynamics.

VI. CONCLUSIONS

We have analysed the overdamped Langevin dynamics of a Brownian particle moving in a multiscale potential. Using multiscale techniques we derived a coarse-grained equation with a space-dependent diffusion tensor (i.e. with multiplicative noise), driven by the system's free energy. The calculation of the diffusion tensor requires the solution of a coupled-system of N Poisson equations. This system can be solved in one dimension and an explicit formula (up to quadratures) for the diffusion coefficient can be obtained.

We demonstrated that the system can exhibit noise/multiscale-induced transitions and these were analyzed in different types of multiscale potentials. In the case of a double well potential with one non-separable microscopic scale, it was shown that the multiscale structure can induce hysteresis effects in the pitchfork bifurcation, something that was observed to be enhanced as the number of microscopic scales was increased. For the case of a tilted three-scale quartic potential we have shown that the presence of the microstructure is able to change the bifurcation diagram such that the resulting effect is that the stability of the zero solution can be tuned by changing the noise intensity. The diffusion coefficient was calculated analytically for a piecewise linear potential at all scales and the transitions in the limit of infinitely many scales were studied.

The present works opens up several new avenues for research. First, the study of noise/multiscale induced transitions in higher dimensions and the construction of the corresponding bifurcation diagram would be a natural extension. Furthermore, it would be interesting to study the effect of inertia on the coarse-grained dynamics. Homogenization problems for the underdamped Langevin dynamics [21] or, even more so, for the generalized

Langevin equation [32] are technically more challenging due to the hypoelliptic nature of the coresponding Fokker-Planck operator. In addition, the study of mean field limits for interacting multiscale diffusions, in the sense of [15] is a very challenging problem. Finally, it would be also interesting to consider the effect of nonreversible perturbations in the multiscale Brownian dynamics. Such a problem is relevant for developing improved sampling techniques for multiscale diffusions [18, 28]. We shall consider these and related issues in future studies.

ACKNOWLEDGMENTS

[1] Assyr Abdulle and Yun Bai. Reduced basis finite element heterogeneous multiscale method for high-order discretizations of elliptic homogenization problems. *Journal of Computational Physics*, 231(21):7014–7036, 2012.

[2] Assyr Abdulle and Yun Bai. Fully discrete analysis of the heterogeneous multiscale method for elliptic problems with multiple scales. *IMA Journal of Numerical Analysis*, page drt066, 2014.

[3] G. Allaire and M. Briane. Multiscale convergence and reiterated homogenisation. *Proc. Roy. Soc. Edinburgh Sect. A*, 126(2):297–342, 1996.

[4] Benjamin T Andrews, Dominique T Capraro, Joanna I Sulkowska, José N Onuchic, and Patricia A Jennings. Hysteresis as a marker for complex, overlapping landscapes in proteins. *The journal of physical chemistry letters*, 4(1):180–188, 2012.

[5] G. Ben Arous and H. Owhadi. Multiscale homogenization with bounded ratios and anomalous slow diffusion. *Comm. Pure Appl. Math.*, 56(1):80–113, 2003.

[6] M. Avellaneda. Iterated homogenization, differential effective medium theory and applications.

Comm. Pure Appl. Math., 40(5):527–554, 1987.

[7] M. T. Barlow and R. F. Bass. The construction of brownian motion on the sierpinski carpet. In *Annales de l'IHP Probabilités et statistiques*, volume 25, pages 225–257, 1989.

[8] R. Battacharya. A central limit theorem for diffusions with periodic coefficients. *The Annals of Probability*, 13:385–396, 1985.

[9] A. Bensoussan, J.-L. Lions, and G. Papanicolaou. *Asymptotic analysis for periodic structures*, volume 5 of *Studies in Mathematics and its Applications*. North-Holland Publishing Co., Amsterdam, 1978.

[10] X. Blanc, C. Le Bris, F. Legoll, and C. Patz. Finite-temperature coarse-graining of one-dimensional models: mathematical analysis and computational approaches. *J. Nonlinear Sci.*, 20(2):241–275, 2010.

[11] A. Bovier and F. den Hollander. *Metastabilty*. Springer-Verlag, 2015. A Potential-Theoretic Approach.

[12] A. Bovier, M. Eckhoff, V. Gayrard, and M. Klein. Metastability in reversible diffusion processes. I. Sharp asymptotics for capacities and exit times. *J. Eur. Math. Soc. (JEMS)*, 6(4):399–424, 2004.

[13] D. Cioranescu and P. Donato. *An Introduction to Homogenization*. Oxford University Press, New York, 1999.

[14] R. David and A. W. Neumann. Contact angle hysteresis on randomly rough surfaces: a computational study. *Langmuir*, 29(14):4551–4558, 2013.

[15] D. A. Dawson. Critical dynamics and fluctuations for a mean-field model of cooperative behavior. *J. Statist. Phys.*, 31(1):29–85, 1983.

[16] A. B. Duncan, C. M. Elliott, G. A. Pavliotis, and A. M. Stuart. A multiscale analysis of diffusions on rapidly varying surfaces. *J. Nonlinear Sci.*, 25(2):389–449, 2015.

[17] A.B. Duncan. Homogenization of Lateral Diffusion on a Random Surface. *Multiscale Model. Simul.*, 13(4):1478–1506, 2015.

[18] A.B. Duncan, T. Lelievre, and G. A. Pavliotis. Variance reduction using nonreversible langevin samplers. *J. Stat. Phys.–to appear*, 2016.

[19] A.B. Duncan and G. A. Pavliotis. Brownian motion in multiscale potentials. *(submitted)*, 2016.

[20] C. W. Gear, J. M. Hyman, P. G. Kevrekidis, I. G. Kevrekidis, O. Runborg, and Theodoropou-

los C. Equation-free, coarse-grained multiscale computation: Enabling microscopic simulators to perform system-level analysis. *Commun. Math. Sci.*, 1:715–762, 2003.

[21] M. Hairer and G. A. Pavliotis. From ballistic to diffusive behavior in periodic potentials. *J. Stat. Phys.*, 131(1):175–202, 2008.

[22] P. Hanggi, P. Talkner, and M. Borkovec. Reaction-rate theory: fifty years after Kramers. *Rev. Modern Phys.*, 62(2):251–341, 1990.

[23] Y. Kadin, Y. Kligerman, and I. Etsion. Unloading an elastic–plastic contact of rough surfaces. *Journal of the Mechanics and Physics of Solids*, 54(12):2652–2674, 2006.

[24] I. G. Kevrekidis and G. Samaey. Equation-free multiscale computation: Algorithms and applications. *Annu. Rev. Phys. Chem.*, 60:321–344, 2009.

[25] S.M. Kozlov. Geometric aspects of averaging. *Uspekhi Mat. Nauk*, 44(2(266)):79–120, 1989.

[26] C. Kuehn. A mathematical framework for critical transitions: Bifurcations, fast-slow systems and stochastic dynamics. *Physica D*, 240(12):1020–1035, 2011.

[27] J. C. Latorre, G. A. Pavliotis, and P. R. Kramer. Corrections to Einstein's relation for Brownian motion in a tilted periodic potential. *J. Stat. Phys.*, 150(4):776–803, 2013.

[28] T. Lelievre, F. Nier, and G. A. Pavliotis. Optimal non-reversible linear drift for the convergence to equilibrium of a diffusion. *J. Stat. Phys.*, 152(2): 237–274 , 2013.

[29] M.C. Mackey, A. Longtin, and A. Lasota. Noise-induced global asymptotic stability. *J. Statist. Phys.*, 60(5-6):735–751, 1990.

[30] J Mortier, C Rakers, M Bermudez, MS Murgueitio, S Riniker, and G Wolber. The impact of molecular dynamics on drug design: applications for the characterization of ligand-macromolecule complexes. *Drug Discovery Today*, 20(6):686–702, 2015.

[31] It converges exponentially fast to the invariant distribution. Details about the rigorous study of (5) can be found in [19].

[32] M. Ottobre and G. A. Pavliotis. Asymptotic analysis for the generalized Langevin equation. *Nonlinearity*, 24(5):1629–1653, 2011.

[33] H. Owhadi. Anomalous slow diffusion from perpetual homogenization. *Ann. Probab.*, 31(4):1935–1969, 2003.

[34] A. L. Pankratov. On certain time characteristics of dynamical systems driven by noise. *Physics Letters A*, 234(5):329–335, 1997.

[35] A. L Pankratov. Time evolution of averages in dynamical systems driven by noise. *Physics

Letters A, 255(1):17–22, 1999.

[36] G. C. Papanicolaou. Diffusion in random media. In *Surveys in applied mathematics, Vol. 1*, volume 1 of *Surveys Appl. Math.*, pages 205–253. Plenum, New York, 1995.

[37] G. A. Pavliotis. A multiscale approach to Brownian motors. *Phys. Lett. A*, 344:331–345, 2005.

[38] G. A. Pavliotis. *Stochastic processes and applications*, volume 60 of *Texts in Applied Mathematics*. Springer, New York, 2014. Diffusion processes, the Fokker-Planck and Langevin equations.

[39] G. A. Pavliotis and A. M. Stuart. Periodic homogenization for inertial particles. *Phys. D*, 204(3-4):161–187, 2005.

[40] G. A. Pavliotis and A. M. Stuart. Parameter estimation for multiscale diffusions. *J. Stat. Phys.*, 127(4):741–781, 2007.

[41] G. A. Pavliotis and A. Vogiannou. Diffusive transport in periodic potentials: Underdamped dynamics. *Fluct. Noise Lett.*, 8(2):L155–173, 2008.

[42] G.A. Pavliotis and A.M. Stuart. *Multiscale Methods*, volume 53 of *Texts in Applied Mathematics*. Springer, New York, 2008. Averaging and Homogenization.

[43] E. Pollak, A. Auerbach, and P. Talkner. Observations on Rate Theory for Rugged Energy Landscapes. *Biophys. J.*, 95(9):4258–4265, NOV 1 2008.

[44] N. Pottier. Analytic study of a model of diffusion on random comb-like structures. *Il Nuovo Cimento D*, 16(8):1223–1230, 1994.

[45] M. Pradas, G. A. Pavliotis, S. Kalliadasis, D. T. Papageorgiou, and D. Tseluiko. Additive noise effects in active nonlinear spatially extended systems. *European Journal of Applied Mathematics*, 23:563–591, 2012.

[46] M. Pradas, N. Savva, J.B. Benjiger, I.G. Kevrekidis, and S. Kalliadasis. Dynamics of fattening and thinning 2d sessile droplets. *Langmuir*, 32:4736–4745, 2016.

[47] M. Pradas, D. Tseluiko, S. Kalliadasis, D. T. Papageorgiou, and G. A. Pavliotis. Noise induced state transitions, intermittency, ans universality in the noisy Kuramoto-Sivashinsky equation. *Physical Review Letters*, 106:060602–, 2011.

[48] N. Savva, G. A. Pavliotis, and S. Kalliadasis. Contact lines over random topographical substrates. part 1. statics. *J. Fluid Mech.*, 672:358–383 , 2011.

[49] N. Savva, G. A. Pavliotis, and S. Kalliadasis. Contact lines over random topographical substrates. part 2. dynamics. *J. Fluid Mech.*, 672:384–410, 2011.

[50] Nikos Savva, Serafim Kalliadasis, and Grigorios A. Pavliotis. Two-dimensional droplet spreading over random topographical substrates. *Phys. Rev. Lett.*, 104(8):084501, Feb 2010.

[51] M. Schmuck, G. A. Pavliotis, and S. Kalliadasis. Effective macroscopic interfacial transport equations in strongly heterogeneous environments for general homogeneous free energies. *Appl. Math. Lett.*, 35:12–17, 2014.

[52] M. Schmuck, M. Pradas, G. A. Pavliotis, and S. Kalliadasis. Upscaled phase-field models for interfacial dynamics in strongly heterogeneous domains. *Proc. R. Soc. A*, 468(2147):3705–3724, 2012.

[53] M. Schmuck, M. Pradas, G. A. Pavliotis, and S. Kalliadasis. Derivation of effective macroscopic Stokes-Cahn-Hilliard equations for periodic immiscible flows in porous media. *Nonlinearity*, 26(12):3259–3277, 2013.

[54] P. N. Sen, C. Scala, and M. H. Cohen. A self-similar model for sedimentary rocks with application to the dielectric constant of fused glass beads. *Geophysics*, 46(5):781–795, 1981.

[55] S. Sriraman, I. G. Kevrekidis, and G. Hummer. Coarse nonlinear dynamics and metastability of filling-emptying transitions: water in carbon nanotubes. *Physical review letters*, 95(13):130603, 2005.

[56] T. Threlfall. Crystallisation of polymorphs: Thermodynamic insight into the role of solvent. *Org. Proc. Res. Dev.*, 4:384–390, 2000.

[57] R. Vellingiri, N. Savva, and S. Kalliadasis. Droplet spreading on chemically heterogeneous substrates. *Phys. Rev. E*, 84:036305, 2011.

[58] C. Wylock, M. Pradas, B. Haut, C. Colinet, and S. Kalliadasis. Disorder-induced hysteresis and nonlocality of contact line motion in chemically heterogeneous microchannels. *Phys, Fluids*, 24:032108, 2012.

[59] R. Zwanzig. Diffusion in a rough potential. *Proc. Natl. Acad. Sci. USA*, 85:2029–2030, 1988.

[60] It converges exponentially fast to the invariant distribution. Details about the rigorous study of (5) can be found in [19].

Appendix A: Brownian motion in an $N-$scale potential: Derivation of the homogenized equation

Consider the following $\mathbb{R}^d-$valued overdamped Langevin diffusion process corresponding to the multiscale potential V^ϵ:

$$dx_t^\epsilon = -\nabla V^\epsilon(x_t^\epsilon)\, dt + \sqrt{2\sigma}\, dW_t, \tag{A1}$$

where W_t is a d-dimensional standard Brownian motion, and where the $N-$scale potential V^ϵ satisfies

$$V^\epsilon(x) = V(x, x/\epsilon, x/\epsilon^2, \ldots, x/\epsilon^N), \tag{A2}$$

for some smooth $V : \mathbb{R}^d \times \mathbb{T}^d \times \ldots \times \mathbb{T}^d \to \mathbb{R}$. Given a smooth observable $f : \mathbb{R}^d \to \mathbb{R}$, the time evolution of the expectation $F^\epsilon(x,t) = \mathbb{E}_{x_0^\epsilon = x}\left[f(x^\epsilon(t)) \right]$ satisfies the following backward Kolmogorov equation (BKE)

$$\partial_t F^\epsilon(x,t) = \mathcal{L}^\epsilon F^\epsilon(x,t), \tag{A3}$$

where the operator $\mathcal{L}^\epsilon$ is the infinitesimal generator $\mathcal{L}^\epsilon$ is defined by

$$\mathcal{L}^\epsilon f(x) = -\nabla V^\epsilon(x) \cdot \nabla f(x) + \sigma \Delta f(x), \quad f \in C_0^2(\mathbb{R}^d).$$

We shall use reiterated homogenization to identify the behaviour of $F^\epsilon(x,t)$ in the limit as $\epsilon \to 0$. We shall follow the formal approach described in [9, Section 3.7], namely of "freezing" the scales $x, x/\epsilon, \ldots, x/\epsilon^{N-1}$ and studying the macroscopic effects of the $O(\epsilon^{-N})$ oscillations using classical periodic homogenization. To this end, we shall formally assume that the variable x/ϵ^N is independent from the variables $x, x/\epsilon, \ldots, x/\epsilon^{N-1}$, writing $V^\epsilon(x) = V_N^\epsilon(x, x/\epsilon^N)$, so that

$$\nabla_x V^\epsilon(x) = \left(\nabla_x + \frac{1}{\epsilon^N}\nabla_z \right) V_N^\epsilon(x, z)\Big|_{z=x/\epsilon^N}.$$

We shall look for solutions $F^\epsilon(x,t)$ of the form $F(x, x/\epsilon^N, t)$ where

$$F(x,z,t) = F_0(x,z,t) + \epsilon F_1(x,z,t) + \epsilon^2 F_2(x,z,t) + \ldots. \tag{A4}$$

The Backward Kolmorogov equation can be rewritten as

$$\partial_t F(x,z,t) = -D_N V^\epsilon(x,z) D_N F(x,z,t) + \sigma D_N \cdot D_N F(x,z,t), \tag{A5}$$

28

where $D_N = (\nabla_x + \epsilon^{-N}\nabla_z)$. We now perform a standard homogenization procedure of the above PDE to obtain the effective dynamics in the limit of $\epsilon \to 0$. We substitute this ansatz (A4) in (A5) and consider the leading order terms of the expansion in powers of ϵ^{-1}. The $O(\epsilon^{-2N})$ can be written as

$$\nabla_z \cdot \left(e^{-V_N^\epsilon(x,z)/\sigma} \nabla_z F_0(x,z,t) \right) = 0, \quad z \in \mathbb{T}^d \tag{A6}$$

Since for fixed x, $e^{-V_N^\epsilon(x,z)/\sigma} > 0$ uniformly on $\mathbb{T}^d$, (A6) implies that F_0 does not depend on the fast variable, i.e. $F_0(x,z,t) = F_0(x,t)$, $\forall (x,t) \in \mathbb{R}^d \times [0,\infty)$. The $O(\epsilon^{-N})$ equation is given by

$$\nabla_z \cdot \left(e^{-V_N^\epsilon(x,z)/\sigma} \nabla_z F_1(x,z,t) \right) = -\nabla_z \cdot \left(e^{-V_N^\epsilon(x,z)/\sigma} \right) \partial_x F_0(x,z,t), \quad z \in \mathbb{T}^d. \tag{A7}$$

Let $\theta_N(x,z)$ be the vector valued solution of the following Poisson equation:

$$\nabla_z \cdot \left(e^{-V_N^\epsilon(x,z)/\sigma} \left(\nabla_z \theta_N(x,z) + I \right) \right) = 0, \quad z \in \mathbb{T}^d, \tag{A8}$$

where $(\nabla_z \theta_N)_{ij} = \partial_{z_i} \theta_{N,j}$, for $i,j = 1,\ldots,d$. It is clear that $F_1(x,z,t) = \theta_N(x,z)\nabla_x F_0(x,t)$ satisfies (A7). Finally, consider the $O(1)$ equation given by

$$
\begin{aligned}
\nabla_z \cdot \left(e^{-V_N^\epsilon(x,z)/\sigma} \nabla_z F_2(x,z,t) \right) = &- \nabla_z \cdot \left(e^{-V_N^\epsilon(x,z)/\sigma} \nabla_x F_1(x,z,t) \right) \\
&- \nabla_x \cdot \left(e^{-V_N^\epsilon(x,z)/\sigma} \nabla_z F_1(x,z,t) \right) \\
&- \nabla_x \cdot \left(e^{-V_N^\epsilon(x,z)/\sigma} \nabla_x F_0(x,t) \right) \\
&- \frac{e^{-V_N^\epsilon(x,z)/\sigma}}{\sigma} \partial_t F_0(x,t).
\end{aligned}
$$

A necessary and sufficient condition for F_2 to exist, is that the RHS has integral zero with respect to $e^{-V_N(x,z)} dz$, i.e.

$$
\begin{aligned}
Z_{N-1}(x)\partial_t F(x,t) &= \sigma \nabla_x \cdot \left(\int e^{-V_N^\epsilon(x,z)/\sigma} \nabla_z F_1(x,z,t)\, dz \right) \\
&\quad + \sigma \nabla_x \left(\int e^{-V_N^\epsilon(x,z)/\sigma}\, dz \nabla_x F_0(x,t) \right) \\
&= \sigma \nabla_x \cdot \left(\int e^{-V_N^\epsilon(x,z)/\sigma} (\nabla_z \theta_N + I)\, dz\, \nabla_x F_0(x,t) \right) \\
&= \nabla_x \cdot \left(K_{N-1}(x) \nabla_x F_0(x,t) \right)
\end{aligned}
$$

where

$$Z_{N-1}(x) = \int e^{-V_N^\epsilon(x,z)/\sigma}\, dz,$$

29

and

$$K_{N-1}(x) = \sigma \int e^{-V_N^\epsilon(x,z)/\sigma}(\nabla_z\theta_N(x,z) + I)\, dz.$$

We now repeat the homogenization process, assuming that the $O(\epsilon^{-(N-1)})$ term is independent from the coarser scales, by reintroducing the small scales the above coarse grained PDE. To this end writing

$$Z_{N-1}(x) = Z_{N-1}^\epsilon(x, x/\epsilon^{N-1}), \quad \text{and} \quad K_{N-1}(x) = K_{N-1}^\epsilon(x, x/\epsilon^{N-1}),$$

and $D_{N-1} = (\nabla_x + \frac{1}{\epsilon^{N-1}}\nabla_z)$ the KBE after coarse-graining the $O(\epsilon^{-N})$ fluctuations can be written as

$$\partial_t F^\epsilon(x, z, t) = \frac{\sigma}{Z_{N-1}^\epsilon(x, z)} D_{N-1} \cdot (K_N(x, z)D_{N-1}F^\epsilon(x, z, t)),$$

where $D_{N-1} = (\nabla_X + \frac{1}{\epsilon^{N-1}}\nabla_z)$. This can now be homogenized in an analogous manner. Suppose now that this homogenization process has been repeated k times so that the resulting coarse-grained PDE is given by

$$\partial_t F^\epsilon(x, z, t) = \frac{\sigma}{Z_{N-k}^\epsilon(x, z)} D_{N-k} \cdot \left(K_{N-k}^\epsilon(x, z)D_{N-k}F^\epsilon(x, z, t)\right), \tag{A9}$$

where

$$Z_{N-k}^\epsilon(x, z) = \int \cdots \int e^{-V_{N-k}^\epsilon(x,z,x_{N-k+1},\ldots,x_N)/\sigma} dx_N \ldots dx_{N-k+1}.$$

and

$$K_{N-k}^\epsilon(x, z) = \sigma \int \cdots \int (I+\nabla_{x_N}\theta_N)\ldots(I+\nabla_{x_{N-k}}\theta_{N-k})e^{-V_{N-k}^\epsilon(x,z,x_{N-k+1},\ldots,x_N)} dx_N \ldots, dx_{N-k+1}.$$

and $D_{N-k} = \nabla_x + \frac{1}{\epsilon^{N-k}}\nabla_z$. Once again, we look for solutions of $F^\epsilon(x, z, t)$ of the form

$$F^\epsilon(x, z, t) = F_0(x, z, t) + \epsilon F_1(x, z, t) + \epsilon^2 F_2(x, z, t) + \ldots.$$

Substituting this ansatz in (A9) we obtain leading order equation:

$$\nabla_z \cdot \left(K_{N-k}^\epsilon(x, z)\nabla_z F_0(x, z, t)\right) = 0,$$

and since for fixed $x \in \mathbb{R}^d$, $K_{N-k}^\epsilon(x, z) > 0$ over $\mathbb{T}^d$, it follows that $F_0(x, z, t) = F_0(x, t)$. The next leading order equation is given by

$$\nabla_z \cdot \left(K_{N-k}^\epsilon(x, z)\nabla_z F_1(x, z, t)\right) = -\nabla_z \cdot \left(K_{N-k}^\epsilon(x, z)\nabla_x F_0(x, z, t)\right). \tag{A10}$$

Letting θ_{N-k} be the solution of the cell equation

$$\nabla_z \cdot \left(K_{N-k}^\epsilon(x,z)\left(\nabla_z\theta_{N-k}(x,z)+I\right)\right) = 0, \tag{A11}$$

then choosing $F_1(x,z,t) = \theta_{N-k}(x,z)\nabla_x F_0(x,t)$ satisfies (A10). The next equation in the expansion is then given by

$$\begin{aligned}
\nabla_z \cdot \left(K_{N-k}^\epsilon(x,z)\nabla_z F_2(x,z,t)\right) = &-\nabla_z \cdot \left(K_{N-k}^\epsilon(x,z)\nabla_x F_1(x,z,t)\right) \\
&- \nabla_x \cdot \left(K_{N-k}^\epsilon(x,z)\nabla_z F_1(x,z,t)\right) \\
&- \nabla_x \cdot \left(K_{N-k}^\epsilon(x,z)\nabla_x F_0(x,t)\right) \\
&- Z_{N-k}^\epsilon(x,z)\partial_t F_0(x,t).
\end{aligned}$$

A necessary and sufficient condition for F_2 to exist is that the RHS has integral zero with respect to $Z_{N-k}^\epsilon(x,z)\,dz$, i.e.

$$\int Z_{N-k}^\epsilon(x,z)\,dz\partial_t F_0(x,t) = \nabla_x \cdot \left(\int K_{N-k}^\epsilon(x,z)\left(\nabla_z\theta_{N-k}(x,z)+I\right)\nabla_x F_0(x,t)\right)$$

Denote by

$$Z_{N-k-1}^\epsilon(x) = \int Z_{N-k}^\epsilon(x,z)\,dz = \int \ldots \int e^{-V_{N-k}^\epsilon(x,x_{N-k},x_{N-k+1},\ldots,x_N)/\sigma}\,dx_{N-k}\,dx_{N-k+1},\ldots,dx_N.$$

We can then choose

$$K_{N-k-1}^\epsilon(x) := \int K_{N-k}^\epsilon(x,z)\left(\nabla_z\theta_{N-k}(x,z)+I\right)\,dz,$$

so that the PDE after coarse graining the $(N-k-1)^{th}$ scale becomes

$$\partial_t F_0(x,t) = \frac{1}{Z_{N-k-1}(x)}\nabla_x \cdot \left(K_{N-k-1}(x)\nabla_x F_0(x,t)\right).$$

Following the above inductive scheme N times, we obtain the following coarse grained PDE which is independent of ϵ:

$$\partial_t F^0(x,t) = \frac{1}{Z(x)}\nabla_x \cdot \left(K(x)\nabla_x F^0(x,t)\right), \tag{A12}$$

where

$$Z(x) = \int \ldots \int e^{-V(x,x_1,\ldots,x_N)/\sigma}\,dx_1\ldots dx_N,$$

and

$$K(x) = \sigma\int \ldots \int \prod_{i=N}^1 (1+\nabla_{x_i}\theta_i(x,x_1,\ldots,x_i))e^{-V(x,x_1,\ldots,x_N)/\sigma}\,dx_N\ldots dx_1,$$

31

where the correctors $\theta_1, \ldots, \theta_N$ are the solutions (known up to additive constants) of (A11).

We can observe that (A12) corresponds to the BKE of a diffusion process x^0 described by the following SDE:

$$dx_t^0 = [-\mathcal{M}(x_t^0)\nabla_x \Psi(x_t^0) + \nabla_x \cdot \mathcal{M}(x_t^0)]\, dt + \sqrt{2\mathcal{M}(x_t^0)}dW_t, \tag{A13}$$

where we have defined:

$$\mathcal{M}(x) = \frac{K(x)}{Z(x)} \tag{A14}$$

and

$$\Psi(x) = -\log Z(x), \tag{A15}$$

One can moreover show that the matrix $\mathcal{M}(x)$ is symmetric positive definite, and therefore a matrix square root $\sqrt{\mathcal{M}(x)}$ is guaranteed to exist.

This result suggests that the process x_t^ϵ converges weakly to x_t^0 as $\epsilon \to 0$. In [19] this convergence is obtained rigorously, subject to assumptions on the range of the multiscale fluctuations arising from V^ϵ.

Appendix B: Calculation of the Effective Diffusion Coefficient in one dimension

In general, one is not able to obtain explicit expressions for the coefficients of the coarse-grained SDE, and one typically must resort to computational methods to approximate $M(x)$, for example solving for $\theta_1, \ldots, \theta_N$ using a numerical PDE solver. However, in the particular case when $d = 1$, we can obtain closed-form solutions for the cell equations, from which the effective diffusion coefficient can be readily calculated. Indeed, the cell equation for the corrector θ_N in one dimension is given by

$$\partial_{x_N}\left(e^{-V(x_0,x_1,\ldots,x_N)/\sigma}\left(\partial_{x_N}\theta_N + 1\right)\right) = 0,$$

so that

$$\partial_{x_N}\theta_N(x_0,\ldots,x_N) + 1 = C(x_0,\ldots,x_{N-1})e^{V(x_0,\ldots,x_N)/\sigma},$$

where

$$C(x_0,\ldots,x_{N-1}) = \left(\int_{\mathbb{T}} e^{V(x_0,\ldots,x_N)/\sigma}\, dx_N\right)^{-1}.$$

The effective diffusion coefficient $\mathcal{K}_{N-1}$ obtained after homogenizing the Nth scale is then given by

$$\mathcal{K}_{N-1}(x_0,\ldots,x_{N-1}) = \sigma \int_{\mathbb{T}} (1 + \partial_{x_N}\theta_{x_N}(x_0,\ldots,x_N))\,dx_N = \sigma \left(\int_{\mathbb{T}} e^{V(x_0,\ldots,x_N)/\sigma}\,dx_N\right)^{-1}.$$

Proceeding inductively from N to 1, if we assume that $\mathcal{K}_{N-k}$ has the form

$$\mathcal{K}_{N-k}(x_0,\ldots,x_{N-k}) = \sigma \left(\int_{\mathbb{T}}\cdots\int_{\mathbb{T}} e^{V(x_0,\ldots,x_N)/\sigma}\,dx_N\ldots,dx_{N-k+1}\right)^{-1},$$

then

$$1 + \partial_{x_{N-k}}\theta_{N-k}(x_0,\ldots,x_{N-k}) = C(x_0,\ldots,x_{N-k-1})\mathcal{K}_{N-k}^{-1}(x_0,\ldots,x_{N-k})$$

where

$$C(x_0,\ldots,x_{N-k-1}) = \left(\int \mathcal{K}_{N-k}(x_0,\ldots,x_{N-k})^{-1}\,dx_{N-k}\right)^{-1}$$

so that

$$\begin{aligned}
\mathcal{K}_{N-k-1}(x_0,\ldots,x_{N-k-1}) &= \int \mathcal{K}_{N-k}(x_0,\ldots,x_{N-k})\left(\theta_{x_{N-k}}(x_0,\ldots,x_{N-k})+1\right)\,dx_{N-k} \\
&= \sigma\left(\int_{\mathbb{T}}\cdots\int_{\mathbb{T}} e^{V(x_0,\ldots,x_N)/\sigma}\,dx_N\ldots,dx_{N-k}\right)^{-1} \\
&= \sigma\left(\int_{\mathbb{T}}\cdots\int_{\mathbb{T}} e^{V(x_0,\ldots,x_N)/\sigma}\,dx_N\ldots dx_{N-k}\right)^{-1}.
\end{aligned}$$

Continuing this procedure inductively, it follows that the effective diffusion coefficient $\mathcal{M}(x) = Z(x)^{-1}\mathcal{K}_1(x)$ can be written as

$$\mathcal{M}(x) = \frac{\sigma}{Z(x)\hat{Z}(x)}, \tag{B1}$$

where

$$\hat{Z}(x) = \int\cdots\int e^{V(x,x_1,\ldots,x_N)/\sigma}\,dx_1\ldots dx_N.$$

In the special case where the scales in the potential are completely separated, i.e. when

$$V^{\epsilon}(x) = V_0(x) + V_1(x/\epsilon) + \ldots + V_N(x/\epsilon^N),$$

for a smooth confining potential V_0 and smooth periodic functions $V_1,\ldots,V_N$, then one can see from (B1) that the effective diffusion coefficient $\mathcal{M}(x)$ tensorises into a product of the form

$$\mathcal{M}(x) = \sigma \prod_{i=1}^{N}\left(\int_{\mathbb{T}} e^{-V_i(y_i)/\sigma}\,dy_i \int_{\mathbb{T}} e^{V_i(z_i)/\sigma}\,dz_i\right)^{-1}. \tag{B2}$$

The contribution of each scale to the potential satisfies

$$\int_{\mathbb{T}} e^{-V_i(u_i)/\sigma}\, du_i \int_{\mathbb{T}} e^{V_i(v_i)/\sigma}\, dv_i \geq \left(\int_{\mathbb{T}} e^{(V_i(u_i) - V_i(u_i))/\sigma}\, du_i \right)^2 = 1,$$

by the Cauchy Schwartz inequality, with equality holding only when $V_i = 0$. This implies that that adding increasingly fine scale fluctuations to V^ϵ will always decrease the effective diffusion coefficient, as one would expect.